

# RSC Advances



This is an *Accepted Manuscript*, which has been through the Royal Society of Chemistry peer review process and has been accepted for publication.

*Accepted Manuscripts* are published online shortly after acceptance, before technical editing, formatting and proof reading. Using this free service, authors can make their results available to the community, in citable form, before we publish the edited article. This *Accepted Manuscript* will be replaced by the edited, formatted and paginated article as soon as this is available.

You can find more information about *Accepted Manuscripts* in the [Information for Authors](#).

Please note that technical editing may introduce minor changes to the text and/or graphics, which may alter content. The journal's standard [Terms & Conditions](#) and the [Ethical guidelines](#) still apply. In no event shall the Royal Society of Chemistry be held responsible for any errors or omissions in this *Accepted Manuscript* or any consequences arising from the use of any information it contains.

# Fabrication of Quasi-cubic Fe<sub>3</sub>O<sub>4</sub>@rGO Composite via Colloid Electrostatic Self-assembly Process for Supercapacitors†

Tiezhu Liu,<sup>a</sup> Xudong Zhang,<sup>a</sup> Baojun Li,<sup>a</sup> Jie Ding,<sup>a</sup> Yushan Liu,<sup>\*a</sup> Ge Li,<sup>a</sup> Xianghe Meng,<sup>a</sup> Qiang Cai<sup>b</sup> and Jianmin Zhang<sup>\*a</sup>

Received (in XXX, XXX) Xth XXXXXXXXX 20XX, Accepted Xth XXXXXXXXX 20XX  
DOI: 10.1039/b000000x

Quasi-cubic Fe<sub>3</sub>O<sub>4</sub>@rGO composite (CFGC) was facilely fabricated to investigate its supercapacitor performance, based on a colloid electrostatic self-assembly process between positively charged Fe(OH)<sub>3</sub> colloid nanoparticles and the negatively charged GO sheets. Scanning electron microscopy (SEM) and transmission electron microscopy (TEM) showed that quasi-cubic Fe<sub>3</sub>O<sub>4</sub> nanoparticles with a diameter of about 10–20 nm were loaded onto the surface of reduced graphene oxide (rGO), which was also characterized with X-ray photoelectron spectroscopy (XPS), Fourier transform infrared spectroscopy (FT-IR), X-ray diffraction (XRD) analyzer. Interestingly, CFGC exhibited the admirable rate property with a high capacitance of 216.7 F g<sup>-1</sup> in 6 M KOH aqueous electrolyte that could be used as electrode material for the superior supercapacitor.

## 1. Introduction

Since the 21st century, energy issues have been the "sword of Damocles", prompting people to research new types of clean, powerful, renewable energy resources. On the other hand, it is also the general trend to develop the environment-friendly and vigorous energy storage devices, such as supercapacitors,<sup>1–5</sup> due to their high power density, rapid charge/discharge time, and long cycling life. Recently, graphene, the well-known one-atom-thick carbon material, has attracted tremendous interest in the energy storage application arena,<sup>6–7</sup> because of its inherent advantages of excellent thermal and electronic conductivity, and large specific surface area (2630 m<sup>2</sup>/g) that can lead theoretically to a capacitor of 550 F/g. As expected, the planar graphene oxide (GO) or reduced graphene oxide (rGO) becomes one ambitious scaffold of the functional nanocomposite for supercapacitors.<sup>8–11</sup> Especially, graphene has been composited with various kinds of metal oxide nanoparticles (NPs)<sup>12–16</sup> to prepare nanostructured hybrid carbonaceous materials for superior supercapacitors, exhibiting enhanced capacitive behaviors with better reversible charging/discharging ability and higher capacitance values.<sup>17–19</sup> Among these inorganic NPs, Fe<sub>3</sub>O<sub>4</sub> is low-cost, non-toxic and environmentally benign,<sup>5–7</sup> indicating that it is a good choice for energy devices; however, its insulating nature hinders its usage in supercapacitors.<sup>20–21</sup> Normally, Fe<sub>3</sub>O<sub>4</sub> NPs combined with conductive graphene is a facile method to significantly decrease the resistance of the materials,<sup>22–27</sup> making it an ideal candidate for supercapacitor electrode materials.<sup>28</sup> At the same time, the intercalated Fe<sub>3</sub>O<sub>4</sub> NPs in such a composite can effectively impede the restacking of graphene sheets,<sup>29</sup> which enhances the specific surface area and pore volume to modify the

property of supercapacitor.<sup>30–34</sup>

In common, only the NPs adjacent to the conductive substrate could participate in the charge/discharge process,<sup>35</sup> hence, the utilization of NPs was low in graphene-based composites and Fe<sub>3</sub>O<sub>4</sub> NPs was no exception, which was unbeneficial for the improvement of electrochemical performance. To further improve performance, many attempts have been adopted to increase the utilization of NPs, such as encapsulation of NPs with graphene,<sup>36–38</sup> decrease the sizes of NPs,<sup>39</sup> adding conductive materials,<sup>35</sup> construct the 3D conductive network,<sup>11</sup> and so on. In comparison with spherical Fe<sub>3</sub>O<sub>4</sub> NPs, quasi-cubic Fe<sub>3</sub>O<sub>4</sub> NPs<sup>25, 40–41</sup> favorably hold the increasingly effective contact area between the graphene plane and Fe<sub>3</sub>O<sub>4</sub> NPs, which leads to the decreasing frequency dependence of ion transport in the electrolyte to the electrode surface. Thereupon, it can be speculated that the hybridization between small quasi-cubic Fe<sub>3</sub>O<sub>4</sub> NPs and conductive graphene substrate will generate a novel composite with excellent electrochemical performance.<sup>36–38</sup> Currently, the combination between Fe<sub>3</sub>O<sub>4</sub> NPs and graphene was achieved by two existing methods,<sup>6–7</sup> in-situ growth and ex-situ assembly, although either surface modification for ex-situ assembly process<sup>6–7, 42</sup> or the excessive NPs produced during in-situ growth process<sup>6–7, 25, 43</sup> inevitably made the whole process complicated. In this paper, we propose a novel simple method to fabricate the quasi-cubic Fe<sub>3</sub>O<sub>4</sub> NPs/reduced graphene oxide (CFGC) induced by a colloid electrostatic self-assembly process between positively charged Fe(OH)<sub>3</sub> colloid NPs and negatively charged GO nanosheets. In the following hydrothermal treatment in an autoclave, the formation of quasi-cubic Fe<sub>3</sub>O<sub>4</sub> NPs and reduction of GO to rGO occurred simultaneously in this process. Furthermore, this CFGC composite exhibits excellent

performance for the potential application for supercapacitors.

## 2. Experimental Section

**Chemicals.** Natural graphite flake with the average diameter of 200 mesh was purchased from Sigma-Aldrich, and used without further purification. Potassium permanganate (KMnO<sub>4</sub>), sodium borohydride (NaBH<sub>4</sub>), potassium hydroxide (KOH), toluene, ethanol, ferric chloride hexahydrate (FeCl<sub>3</sub>·6H<sub>2</sub>O), hydrogen peroxide (H<sub>2</sub>O<sub>2</sub>) and concentrated sulphuric acid (H<sub>2</sub>SO<sub>4</sub>, 98%) were analytical grade reagent received from Tianjin Chemical (Tianjin, China). Deionized water was used throughout the experiments.

**Synthesis of CFGC.** Positively charged Fe(OH)<sub>3</sub> colloid solution was prepared by the method in literature.<sup>38</sup> GO powder was synthesized by the modified Hummers' method.<sup>44</sup> At first, after 50 mg GO powder added into 500 mL deionized water was ultrasonicated for 30 min to obtain the GO suspension, 10.7 mL Fe(OH)<sub>3</sub> colloid was added dropwisely into such stirred GO suspension. The brown precipitate generated slowly and the mixed suspension was gradually transparent. When the suspension was totally colorless and transparent, the brown Fe(OH)<sub>3</sub>/GO composite was obtained after centrifugation and dried at 60 °C in vacuum oven overnight. Hereafter, the powder composite was treated in a hydrothermal treatment process in autoclave at 120 °C for 4 h. Finally, the magnetic black powder product was gained and named as quasi-cubic Fe<sub>3</sub>O<sub>4</sub>/rGO composite (CFGC).

**Materials Characterization.** Fourier transform infrared (FT-IR) spectroscopic measurements were conducted by using a Bruker IFS 66 v s<sup>-1</sup> infrared spectrometer. Raman spectra were recorded on a Renishaw RM-1000 instrument with excitation from the 514 nm line of an Ar ion laser with a power of about 5 mW. The phase structures of samples were characterized with X-ray diffraction (XRD, Bruker D8 advance) with Cu Kα radiation (λ = 1.5418 Å). The X-ray photoelectron spectra (XPS) of CFGC was obtained by a PHI-5702 multi-functional X-ray photoelectron spectrometer (Physical Electronics Inc., Chanhassen, MN, USA) with pass energy of 29.35 eV and an Mg Ka line excitation source, while the binding energy of C 1s (284.6 eV) was used. The surface morphologies of composites were observed by using a JEOL JSM-6301F instrument. The transmitting electron microscopy (TEM) pattern was performed on a JEOL JEM-2010F electron microscope (Japan) operating at 200 kV. The powder samples were dispersed in water in an ultrasonic bath for 5 min, and deposited on a copper grid covered with a perforated carbon film.

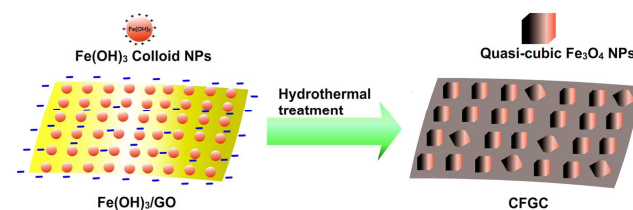
**Electrochemical Measurement.** The CFGC composite electrodes were prepared for supercapacitor measurement as follows: a mixture containing 80 wt % active materials (3 mg), 10 wt % carbon black, and 10 wt % polytetrafluoroethylene (PTFE) was well mixed in N,N-dimethylformamide (DMF) until they formed a slurry with the proper viscosity, and then the slurry was uniformly laid on a piece of Ni foam about 1 cm<sup>2</sup> that was used as a current collector and then dried at 50 °C for 24 h. The Ni foam coated with the CFGC composite was pressed for 1 min under 1.0

55 MPa. The electrochemical behavior of the composite electrode was evaluated by cyclic voltammetry (CV), electrochemical impedance spectroscopy (EIS) and galvanostatic charge-discharge. Respectively, Cyclic voltammetry (CV) was conducted with a CHI660C electrochemical workstation with voltage scan rates of 5, 10, 20, 50, 80 and 100 mV s<sup>-1</sup>. Electrochemical impedance spectroscopy (EIS) was performed with a CHI660C electrochemical workstation in a frequency range from 100 kHz to 1 Hz at open circuit potential. CV and EIS tests were performed in a three-electrode glass cell, a platinum counter electrode, and a standard calomel reference electrode (SCE). The galvanostatic charge-discharge tests were conducted on a LAND battery system at the current densities of 0.5, 1.0, 2.0, 3.0 and 5 A g<sup>-1</sup>. The average specific capacitance was estimated from the discharge slope according to the following equation:

$$C = I\Delta t / (\Delta V \times m)$$

Where *C* is specific capacitance, *I* is the current loading (A),  $\Delta t$  is the discharge time (s),  $\Delta V$  is the potential change during discharge process, and *m* is the mass of active material in a single electrode (g).

## 3. Results and discussions



**Scheme 1.** Construction process of CFGC.

In common, the positively charged colloidal Fe(OH)<sub>3</sub> nanoparticles is prepared via an hydrolysis process of FeCl<sub>3</sub>,<sup>38</sup> and GO sheets obtained by the Hummers' method<sup>44</sup> show the negatively charged surfaces. Hence, the Fe(OH)<sub>3</sub> colloidal nanoparticles would be easily assembled onto the GO sheets by the strong electrostatic interactions, which was observed in the TEM images of Fe(OH)<sub>3</sub>/GO composite (Fig. S1). In addition, such self-assembly process can be further stabilized by the other noncovalent (van der Waals interactions and hydrogen bonding) interactions as well as chemisorptions between the Fe(OH)<sub>3</sub> colloid nanoparticles and the carboxylic, hydroxyl, and epoxy groups present on the GO surface.<sup>15, 36, 38</sup>

As shown in Scheme 1, when birck-red Fe(OH)<sub>3</sub> colloid aqueous solution was added into the yellow GO aqueous suspension, the brown particulate appeared slowly and the suspension was gradually transparent, indicating that the positive Fe(OH)<sub>3</sub> colloid nanoparticles was incorporated with the negative GO sheets. Subsequently, the Fe(OH)<sub>3</sub>/GO composite was obtained by centrifugation, and followed an hydrothermal treatment in an autoclave at 120 °C by using NaBH<sub>4</sub> as reducing agent. Under such condition, quasi-cubic Fe<sub>3</sub>O<sub>4</sub> nanoparticles and rGO were obtained simultaneously to totally convert into the desired product CFGC.

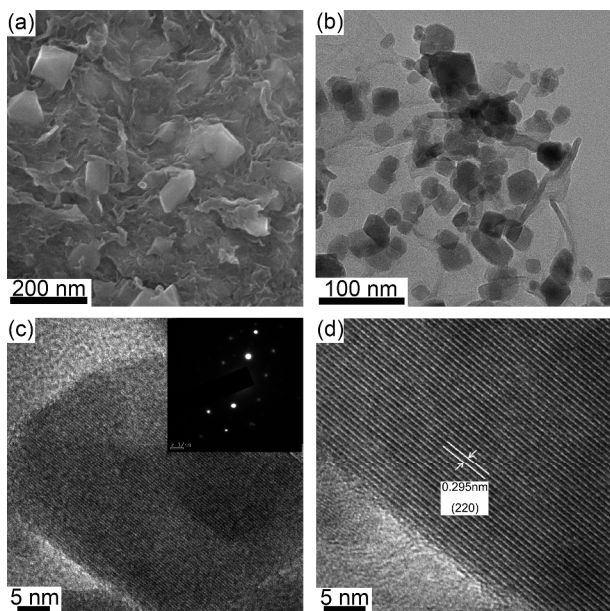


**Fig.1** (a) SEM image of CFGC, (b) TEM image of CFGC, (c) and (d) HRTEM images of CFGC.

In this work, SEM, TEM, HR-TEM, FT-IR, Raman, XRD and XPS measurements are generally used to confirm the identity of CFGC. As shown in Fig. 1a, SEM image clearly shows the quasi-cubic  $\text{Fe}_3\text{O}_4$  NPs dispersed onto the curved thin flaky layer-like rGO sheets uniformly. At the same time, TEM photographs of the sample (Fig. 1b and Fig. S2) obviously manifested that the morphology of the composite material was almost consistent with the rGO sheets in the range of micrometers. Meanwhile,  $\text{Fe}_3\text{O}_4$  nanoparticles mainly loaded onto the surface or intercalate between the rGO sheets. Evidently, no alone quasi-cubic  $\text{Fe}_3\text{O}_4$  NPs or rGO nanosheet is observed, roughly indicating the self-assembly process between the  $\text{Fe}(\text{OH})_3$  colloidal nanoparticles and GO nanosheets, which is consistent with the result from the TEM images of  $\text{Fe}(\text{OH})_3/\text{GO}$  composite (Fig S1). Interestingly, the morphology of the  $\text{Fe}_3\text{O}_4$  NPs anchored onto rGO is quasi-cubic with diameter of about 10-30 nm, completely different with the spherical  $\text{Fe}(\text{OH})_3$  colloid particles (Fig. S1). This is possibly ascribed by that the adjacent  $\text{Fe}(\text{OH})_3$  colloidal nanoparticles loaded onto the GO sheets reassembly and generate the quasi-cubic  $\text{Fe}_3\text{O}_4$  NPs during the hydrothermal treatment process. This result also confirmed the combination between rGO and quasi-cubic  $\text{Fe}_3\text{O}_4$  NPs, which was coherent with the interpretation of SEM experiment. Also, the as-prepared quasi-cubic  $\text{Fe}_3\text{O}_4$  NPs are highly ordered crystals, which can be confirmed from the six fine diffraction spots observed from the corresponding SAED pattern (inset in Fig. 1c).<sup>45</sup> The detailed structure of the quasi-cubic  $\text{Fe}_3\text{O}_4$  NPs is shown in Fig. 1d. The distinctly resolved lattice observed from HRTEM is measured to be around 0.295 nm that corresponds to the (220) plane of quasi-cubic  $\text{Fe}_3\text{O}_4$  NPs.<sup>46</sup>

Depicted by Fig. 2a, the FT-IR spectra also displays the presence of rGO and  $\text{Fe}_3\text{O}_4$ , as well as their combination in the CFGC. Visibly, the broad characteristic band in the range of 3500–3300  $\text{cm}^{-1}$  can be assigned to O–H stretching vibrations arising from hydroxyl groups of the GO sheets, and water adsorbed in the GO

sheets, which disappeared in those of rGO and CFGC. Meanwhile, no stretching vibration of carboxyl groups (1723  $\text{cm}^{-1}$ ) or epoxide groups (1093  $\text{cm}^{-1}$ ) was observed, remarking the completed reduction of GO to rGO.<sup>15, 16</sup> The very weak peaks at around 2936 and 2854  $\text{cm}^{-1}$  can be assigned to the asymmetric and symmetric vibrations of C–H, respectively.<sup>15, 16</sup> Furthermore, the vibration at 1571  $\text{cm}^{-1}$  can be assigned to the stretching vibration of C=C of rGO and another at 1086  $\text{cm}^{-1}$  can be assigned to the stretching vibration of C–O of rGO.<sup>34</sup> Compared by  $\text{Fe}_3\text{O}_4$  (Fig. 2a: ii), in case CFGC, the typical vibrations of the  $\text{Fe}^{2+}\text{--O}^{2-}$  and  $\text{Fe}^{3+}\text{--O}^{2-}$  also were observed at 567 and 416  $\text{cm}^{-1}$ , respectively, which was consistent with the reported IR spectrum of spinel bulk  $\text{Fe}_3\text{O}_4$ .<sup>39, 47</sup> Herein, the Raman spectra of the CFGC, rGO and GO investigated with  $\text{Ar}^+$  laser excitation (514.5 nm) were described in Fig. 2b. For all the samples, the G band (1588  $\text{cm}^{-1}$ ) is corresponding to the  $\text{sp}^2$  hybridized carbon, while the D band (1322  $\text{cm}^{-1}$ ) is originating from the disordered carbon. As shown in Fig. 2b, the intensity ratio of D over G band is higher than that for rGO and GO, which is consistent with the literature.<sup>15, 16</sup> On the other hand, the distinctly increased D band intensity of the CFGC results from the structure interaction between  $\text{Fe}_3\text{O}_4$  NPs and rGO sheets.<sup>30, 39</sup>

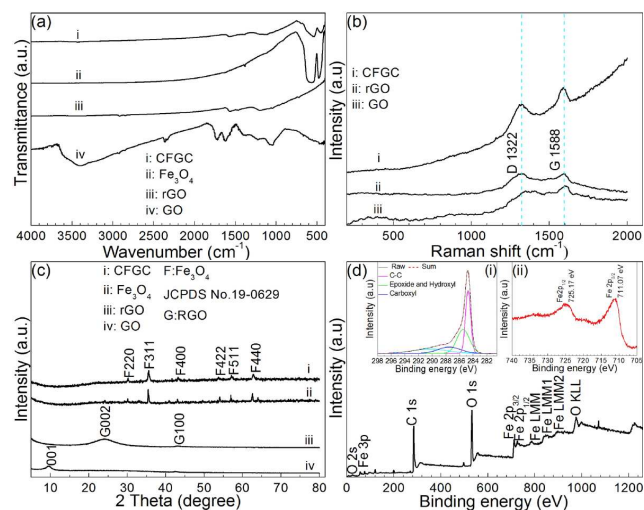


**Fig.2** (a) FT-IR spectra of GO, rGO,  $\text{Fe}_3\text{O}_4$  and CFGC, (b) Raman spectra of GO, rGO, and CFGC (c) XRD patterns of GO, rGO,  $\text{Fe}_3\text{O}_4$  and CFGC, (d) XPS spectra of CFGC. Inset in (d) is the high spectra of C 1s and Fe.

Moreover, the phase structures of the samples (GO, rGO and CFGC) are investigated by the XRD measurements, which were shown in Fig. 2c. The XRD pattern of CFGC illustrated that the positions and relative intensities of the diffraction peaks matched well with standard  $\text{Fe}_3\text{O}_4$  and graphene patterns. As we expect, the weak peaks at 24.3° (002) and 43.6° (100) are attributed to that rGO and the disappearance of the peak at 9.7° (001) corresponding to GO sheets indicates that the GO has been fully reduced to rGO by the heat treatment process.<sup>48</sup> On the other hand, the peaks at 2 $\theta$  values of 30.1° (220), 35.4° (311), 43.0° (400), 53.7° (422), 57.2° (511), and 62.6° (440) are consistent with the standard XRD data for the magnetite phase (JCPDS No. 19–0629).<sup>39, 47</sup>

To obtain further information on the surface composition of CFGC, XPS analysis was executed, which is very sensitive to the

Fe<sup>2+</sup> and Fe<sup>3+</sup> cations. As shown in Fig. 2d, the peaks at 711.07 and 725.17 eV in the high resolution Fe2p scan are ascribed to the levels of Fe2p3/2 and Fe2p1/2 in the CFGC,<sup>39, 49</sup> respectively (inset ii in Fig. 2d). On the other hand, in agreement with the literature, the peaks shift to higher binding energy and broaden for Fe<sub>3</sub>O<sub>4</sub> is owing to the appearance of Fe<sup>2+</sup>(2p3/2) and Fe<sup>2+</sup>(2p1/2). The predominant peak at 531.8 eV is attributed to O1s, which belongs to the lattice oxygen of Fe<sub>3</sub>O<sub>4</sub>, and the weak shoulder peak at around 710 eV provides the further evidence of Fe<sub>3</sub>O<sub>4</sub>.<sup>50</sup> Therefore, the XPS pattern reveals that Fe<sub>3</sub>O<sub>4</sub> has been generated by the reduction of Fe(OH)<sub>3</sub>.<sup>51, 52</sup> For the carbon component in the CFGC, the peak located at 284.6 eV is assigned to the characteristic peak of C1s. The peak at 286.2 eV is attributed commonly to surface-adsorbed hydrocarbons and their oxidative forms (e.g., C–OH and epoxide), while the peak at 288.6 eV in the C1s spectrum (inset i in Fig. 3b) is assigned to the carbon element in association with oxygen in the carbonate ions.<sup>15, 39</sup> The remaining smaller peaks at higher binding energies (785.6, 788.2, 802.1, and 805.2 eV) are satellite shake-ups of the assigned components.

Significantly, before the electrochemical performance study of CFGC for supercapacitor electrode material, N<sub>2</sub> adsorption-desorption isotherms show the type IV based on the notable hysteresis loops, which indicates that CFGC possesses a typical mesoporous structure (Fig.S3a). From the adsorption branch of the isotherm, the specific surface area is calculated of 71.7 m<sup>2</sup> g<sup>-1</sup> by a multi-point Brunauer-Emmett-Teller method, and the most probable pore width is calculated of 5.76 nm in the Barrett-Joyner-Halenda model. In case CFGC, distribution of pore width is concentrated in the range of mesoporous structure (Fig.S3b), the total pore volume is of 0.106 cm<sup>3</sup> g<sup>-1</sup> ranging from 1.7 to 300 nm. The porous structure of CFGC with high surface area and pore volume facilitates electrolyte ion diffusion to active sites with less resistance<sup>53</sup> and acts as a buffer layer for volume expansion<sup>54</sup> of quasi-cubic Fe<sub>3</sub>O<sub>4</sub> during the charge-discharge process. At the same time, the porosity of CFGC could shorten the diffusion paths of ion and electrons. All of these could contribute to fabricate high performance electrode materials for supercapacitors.

As well-known, Fe<sub>3</sub>O<sub>4</sub> NPs is usually super-paramagnetic. The M–H measurements were performed to investigate the behavior of CFGC at room temperature with the magnetic field swept back and forth between 10 and -10 kOe (1 Oe = 10<sup>3</sup>/4π A m<sup>-1</sup> = 79.59 A m<sup>-1</sup>; Ms is the specific saturation magnetization and the Hc is the coercitive field.). The magnetization of the FGC is measured and its saturation magnetization is 23.9 emu g<sup>-1</sup>, as shown in Fig.3, which exhibits typical super-paramagnetic behavior. Compared with bulk magnetite (Ms = 92 emu/g),<sup>55</sup> the Ms value of the FGC particles were lower; this lowering was due to nonmagnetic rGO sheets coated by quasi-cubic Fe<sub>3</sub>O<sub>4</sub> NPs on the surfaces. At the same time, the small Hc (178.7 Oe) means that the sample can be acted as one soft magnetic material. This phenomenon further proves that the Fe<sub>3</sub>O<sub>4</sub> nanoparticles have been successfully loaded on the rGO sheets.

Carbonaceous materials are widely used as electrode materials in supercapacitors, because of their large surface area and high conductivity. Herein, the detailed electrochemical property of CFGC was investigated for its potential application of

supercapacitor. Firstly, as shown in Fig. 3a, the cyclic voltammogram (CV) curves for CFGC at different scan rate at the range from 0.1 V to 0.7 V (vs SCE, Saturated calomel electrode) demonstrate that the features of Fe<sub>3</sub>O<sub>4</sub> pseudocapacitance (Fig. S4a) are remarkably depressed due to the low content of Fe<sub>3</sub>O<sub>4</sub> in the composite,<sup>56</sup> hence, CFGC has slightly difference in the shapes of its CV curves in comparison with rGO and Fe<sub>3</sub>O<sub>4</sub>. Furthermore, the CV curves of CFGC composite are much wider than those of Fe<sub>3</sub>O<sub>4</sub> recorded at the same scan rates, indicating higher specific capacitances.

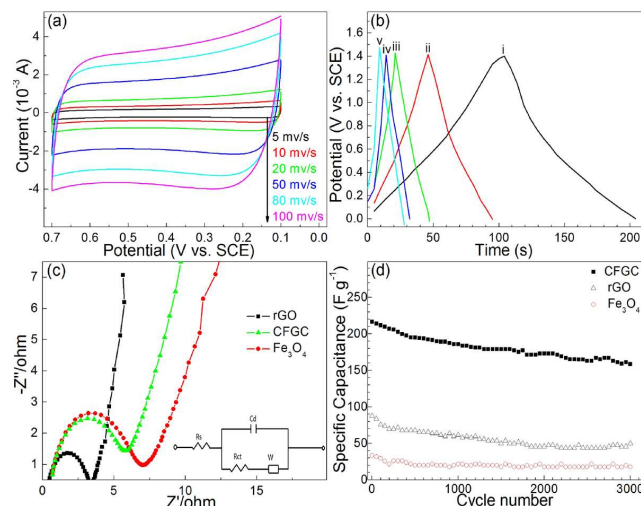


**Fig.3** (a) The cyclic voltammogram (CV) curves of CFGC under the different scan rates of 5, 10, 20, 50, 80, and 100 mV s<sup>-1</sup>; (b) GCD curves of CFGC at different current densities, i: 500 mA g<sup>-1</sup>, ii: 1000 mA g<sup>-1</sup>, iii: 2000 mA g<sup>-1</sup>, iv: 3000 mA g<sup>-1</sup>, v: 5000 mA g<sup>-1</sup>; (c) EIS of rGO, Fe<sub>3</sub>O<sub>4</sub> and CFGC, the inset shows the equivalent Randles circuit; (d) cycling performances of CFGC, rGO and Fe<sub>3</sub>O<sub>4</sub>.

In this paper, the specific capacitance values were obtained from the galvanostatic discharge method, which can directly evaluate the adaptability of the supercapacitor. As shown in Fig. 3b, The specific capacitances were calculated by the corresponding galvanostatic discharge curves in the range of 0 V to 1.4 V at various current densities. The values of pseudocapacitances for Fe<sub>3</sub>O<sub>4</sub>/rGO composite are 216.7 F g<sup>-1</sup> at 0.5 A g<sup>-1</sup>, 194.4 F g<sup>-1</sup> at 1 A g<sup>-1</sup>, 167.0 F g<sup>-1</sup> at 2 A g<sup>-1</sup>, 146.9 F g<sup>-1</sup> at 2 A g<sup>-1</sup> and 144.0 F g<sup>-1</sup> at 5 A g<sup>-1</sup>, respectively. Especially, at a discharge current density of 0.5 A g<sup>-1</sup>, the calculated specific capacitances for CFGC composite is 216.7 F g<sup>-1</sup>, much higher than that of Fe<sub>3</sub>O<sub>4</sub> (87.6 F g<sup>-1</sup>) or rGO (33.5 F g<sup>-1</sup>) shown in Fig. S4c. It is obvious that the capacitance performances of the composite is significantly improved by the synergistic effects between the two components.<sup>57, 58</sup> Detailedly, the high surface area of the CFGC generated from the intercalation of quasi-cubic Fe<sub>3</sub>O<sub>4</sub> NPs in graphene sheets, which could provide more accessible sites for the intercalation and/or absorption of electrons and ions in electrolyte. The as-prepared CFGC actually shows lower capacitance compared with the high performance of reported Fe<sub>3</sub>O<sub>4</sub> @rGO example,<sup>59</sup> which is might be induced by the different measurement conditions and different preparation method adopted. Further exploration are undergoing in our laboratory to improve the current result.

The enhanced capacitive performance in the CFGC may result from the low resistance which is investigated by EIS. As shown

in Fig. 3c, all spectra of Fe<sub>3</sub>O<sub>4</sub>, rGO and CFGC composite are similar in shape, where a semi-circle in the high frequency region and inclined line in the low frequency region are observed. It is known that a large semi-circle for the electrode suggests high interfacial charge-transfer resistance, probably resulting from the poor electrical conductivity of active materials, while the inclined portion is ascribed to the Warburg impedance, which is a consequence of the frequency dependence of ion diffusion/transport in the electrolyte to the electrode surface.<sup>57, 58</sup> Fitting with the Zview program in Sai software set, the values of charge-transfer resistance for rGO, Fe<sub>3</sub>O<sub>4</sub> and CFGC composite are 3.154 Ω, 6.825 Ω and 6.097 Ω, respectively. The reduced charge-transfer resistance for the CFGC electrode would be attributed to the enhanced conductivity of rGO support. The intersecting part with the real axis in the high frequency range is the resistance resulting from the frequency dependence of ion diffusion/transport. The low resistance of ion transfer in the CFGC electrodes may contribute to the high capacitance.<sup>57, 58</sup> Therefore, the EIS data indicate that the electrical conductivity of the CFGC electrode is further improved by the presence of rGO, leading to enhanced electrochemical properties.

To investigate the further performance of novel material CFGC, the cycling stability of the CFGC was tested by conducting continuous charge-discharge cycles at a constant discharge current density of 0.5 A g<sup>-1</sup>. As shown in Fig. 3d, specific capacitance of the CFGC composite electrode decreases from 216.7 F g<sup>-1</sup> to 195.1 F g<sup>-1</sup> during the first 500 cycles and remains stable till 3000th cycle. A serious decline in capacitance during the first 500 cycles is probably contributed to the active materials fell down from the collector. Even so, the capacitance retention exceeded 73.2 % after 3000 cycles (158.6 F g<sup>-1</sup>). This result represents that the high stability of the CFGC is suitable applied for high performance supercapacitor.

#### 4. Conclusions

At consequence, novel material CFGC was designed and prepared by the simple hydrothermal treatment, induced by the colloidal electrostatic self-assembly between the untreated Fe(OH)<sub>3</sub> colloidal particles and negatively charged GO sheets. The co-formation of rGO and quasi-cubic Fe<sub>3</sub>O<sub>4</sub> nanoparticles occurred simultaneously, which resulted in the quasi-cubic Fe<sub>3</sub>O<sub>4</sub> nanoparticles dispersed onto the surface of graphene sheets uniformly. CFGC composite with micrometer size exhibits superparamagnetic property with a Ms of 23.9 emu g<sup>-1</sup>. CFGC also showed superior performance as an electrode material in supercapacitors, which makes CFGC an excellent candidate material for application in energy storage issues. Hence, we believe that this novel method may be one versatile platform for synthesizing other functional graphene/inorganic nanocomposites from colloidal solution in the future.

#### Acknowledgements

Financial was supported from the China Postdoctoral Science Foundation (No. 2013M531681), the National Science Foundation of China (No. 21373189) and the S&T Project of

Education Department of Henan Province of China (No. 13A150597).

#### Notes and references

- <sup>a</sup> College of Chemistry and Molecular Engineering, Zhengzhou University, 100 Science Road, Zhengzhou 450001, P R China. E-mail: liuyushan@zzu.edu.cn and zhjm@zzu.edu.cn
- <sup>b</sup> Key Laboratory for Advanced Materials of Ministry of Education and College of Materials Science and Engineering, Tsinghua University, Beijing 100084, PR China
- <sup>†</sup> Electronic Supplementary Information (ESI) available: Synthesis of graphene oxide, TEM images, SEM images, Magnetization curves, Nitrogen adsorption desorption isotherms, CV and GCD curves. See DOI: 10.1039/b000000x/
- 1 K. Nao, W. Naoi, S. Aoyagi, J. Miyamoto and T. Kamino, *Acc. Chem. Res.*, 2013, **46**, 1075.
  - 2 P. Flynn, Technical Report, National Research Council, 2004.
  - 3 E. Frackowiak and F. Beguin, *Carbon*, 2001, **39**, 937.
  - 4 D. Lozano-Castello, D. Cazorla-Amoros, A. Linares-Solano, S. Shiraishi, H. Kurihara and A. Oya, *Carbon*, 2003, **41**, 1765.
  - 5 C. M. A. Brett, A. M. O. Brett, Oxford University Press Inc, New York 1993, ch. 7.
  - 6 S. Bai and X. P. Shen, *RSC Adv.*, 2012, **2**, 64.
  - 7 S. Xin, Y. G. Guo and L. J. Wan, *Acc. Chem. Res.*, 2012, **45**, 1759.
  - 8 K. S. Novoselov, A. K. Geim, S. V. Morozov, D. Jiang, Y. Zhang, S. V. Dubonos, I. V. Grigorieva and A. A. Firsov, *Science*, 2004, **306**, 666.
  - 9 R. R. Nair, P. Blake, A. N. Grigorenko, K. S. Novoselov, T. J. Booth, T. Stauber, N. M. R. Peres and A. K. Geim, *Science*, 2008, **320**, 1308.
  - 10 C. Lee, X. D. Wei, J. M. Kysar and J. Hone, *Science*, 2008, **321**, 385.
  - 11 A. A. Balandin, S. Ghosh, W. Z. Bao, I. Calizo, D. Teweldebrhan, F. Miao and C. N. Lau, *Nano Lett.*, 2008, **8**, 902.
  - 12 D. P. Dubal, S. H. Lee, J. G. Kim, W. B. Kim and C. D. Lokhande, *J. Mater. Chem.*, 2012, **22**, 3044.
  - 13 Y. Liu, W. Wang, Y. W. Wang, Y. L. Ying, L. W. Sun and X. S. Peng, *RSC Adv.*, 2014, **4**, 16374–16379.
  - 14 L. Mao, K. Zhang, H. S. O. Chan and J. S. Wu, *J. Mater. Chem.*, 2012, **22**, 1845.
  - 15 Y. S. Liu, X. Q. Jiang, B. J. Li, X. D. Zhang, T. Z. Liu, X. S. Yan, J. Ding, Q. Cai and J. M. Zhang, *J. Mater. Chem. A*, 2014, **2**, 4264.
  - 16 C. Z. Yuan, L. H. Zhang, L. R. Hou, G. Pang and Won-Chun Oh, *RSC Adv.*, 2014, **4**, 14408–14413.
  - 17 H. L. Wang, J. T. Robinson, G. Diankov and H. J. Dai, *J. Am. Chem. Soc.*, 2010, **132**, 3270.
  - 18 D. H. Wang, D. W. Choi, J. Li, Z. G. Yang, Z. M. Nie, R. Kou, D. H. Hu, C. M. Wang, L. V. Saraf, J. G. Zhang, I. A. Aksay and J. Liu, *ACS Nano*, 2009, **3**, 907.
  - 19 S. Stankovich, D. A. Dikin, G. H. B. Dommett, K. M. Kohlhaas, E. J. Zimney, E. A. Stach, R. D. Piner, S. T. Nguyen and R. S. Ruoff, *Nature*, 2006, **442**, 282.
  - 20 K. K. Lee, S. Deng, H. M. Fan, S. Mhaisalkar, H. R. Tan, E. S. Tok, K. P. Loh, W. S. Chin and C. H. Sow, *Nanoscale*, 2012, **4**, 2958.
  - 21 B. Subramani, P. P. Muzhikara, A. Srinivasan, R. Dinesh, G. Raghavan and T. R. Narasinga, *Phys. Chem. Chem. Phys.*, 2014, **16**, 5284.
  - 22 Z. Y. Cao and B. Q. Wei, *ACS Appl. Mater. Interfaces*, 2013, **5**, 10246.
  - 23 T. Qi, J. J. Jiang, H. C. Chen, H. Z. Wan, L. Miao and L. Zhang, *Electrochimica Acta*, 2013, **114**, 674.
  - 24 Q. T. Qu, S. B. Yang and X. L. Feng, *Adv. Mater.*, 2011, **23**, 5574–5580.
  - 25 Q. H. Wang, L. F. Jiao, H. M. Du, Y. J. Wang and H. T. Yuan, *J. Power Sources*, 2014, **245**, 101.
  - 26 Y. W. Liu, M. X. Guan, L. Feng, S. L. Deng, J. F. Bao, S. Y. Xie, Z. Chen, R. B. Huang and L. S. Zheng, *Nanotechnology*, 2013, **24**, 025604.
  - 27 D. H. Guan, Z. Gao, W. L. Yang, J. Wang, Y. Yuan, B. Wang, M. L. Zhang and L. H. Liu, *Mater. Sci. Eng. B*, 2013, **178**, 736.

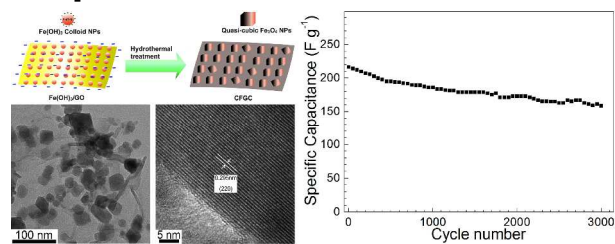
- 28 U. M. Patil, J. S. Sohn, S. B. Kulkarni, S. C. Lee, H. G. Park, K. V. Gurav, J. H. Kim and S. C. Jun, *ACS Appl. Mater. Interfaces*, 2014, **6**, 2448.
- 29 Y. Chen, B. H. Song, M. Li, L. Lu, J. M. Xue, *Adv. Funct. Mater.*, 2014, **24**, 319.
- 30 B. J. Li, H. Q. Cao, G. Yin, Y. X. Lu and J. F. Yin, *J. Mater. Chem.*, 2011, **21**, 10645–10648.
- 31 Y. Wang, Y. J. Bai, X. Li, Y. Y. Feng and H. J. Zhang, *Chem. Eur. J.*, 2013, **19**, 3340–3347.
- 10 32 Z. Wang, C. Y. Ma, H. L. Wang, Z. H. Liu and Z. P. Hao, *J. Alloys Compd.*, 2013, **552**, 486–491.
- 33 M. D. Stoller, S. Park, Y. Zhu, J. An and R. S. Ruoff, *Nano Lett.*, 2008, **8**, 3498–3502.
- 34 M. J. Kim, Y. S. Hwang and J. H. Kim, *J. Power Sources*, 2013, **239**, 225–233.
- 15 35 G. H. Yu, L. B. Hu, N. Liu, H. L. Wang, M. Vosgueritchian, Y. Yang, Y. Cui and Z. N. Bao, *Nano Lett.*, 2011, **11**, 4438–4442.
- 36 S. B. Yang, X. L. Feng, S. Ivanovici and K. Müllen, *Angew. Chem. Int. Ed.*, 2010, **49**, 8408–8411.
- 20 37 W. Wei, S. B. Yang, H. X. Zhou, I. Lieberwirth, X. L. Feng and K. Müllen, *Adv. Mater.*, 2013, **25**, 2909–2914.
- 38 Y. T. Chen, G. Fei, Y. Qiu, H. Hu, I. Kulaots, E. Walsh and R. H. Hurt, *ACS Nano*, 2013, **7**, 3744–3753.
- 39 B. J. Li, H. Q. Cao, J. Shao, M. Z. Qu and J. H. Warner, *J. Mater. Chem.*, 2011, **21**, 5069–5075.
- 25 40 X. T. Zhang, J. Q. Wan, K. Z. Chen and S. X. Wang, *J. Cryst. Growth*, 2013, **372**, 170–174.
- 41 H. Khurshid, W. Li, S. Chandra, M. H. Phan, G. C. Hadjipanayis, P. Mukherjee and H. Srikanth, *Nanoscale*, 2013, **5**, 7942–7952.
- 30 42 M. C. Liu, T. Wen, X. L. Wu, C. L. Chen, J. Hu, J. Li and X. K. Wang, *Dalton Trans.*, 2013, **42**, 14710–14717.
- 43 Q. Zhou, Z. B. Zhao, Z. Y. Wang, Y. F. Dong, X. Z. Wang, Y. Gogotsi and J. S. Qiu, *Dalton Trans.*, 2014, **6**, 2286–2291.
- 44 W. S. Hummers and R. E. Offeman, *J. Am. Chem. Soc.*, 1958, **80**, 1339–1339.
- 35 45 N. N. Guan, D. J. Sun and J. Xu, *Mater. Lett.*, 2009, **63**, 1272–1274.
- 46 Z. H. Xing, S. S. Wang and A. W. Xu, *Cryst. Eng. Comm.*, 2014, **16**, 1482–1487.
- 47 L. L. Ren, H. Y. Wu, M. M. Lu, Y. J. Chen, C. L. Zhu, P. Gao, M. S. Cao, C. Y. Li and Q. Y. Ouyang, *ACS Appl. Mater. Interfaces*, 2012, **4**, 6436–6442.
- 40 48 C. Nethravathi, B. Viswanath, C. Shivakumara, N. Mahadevaiah and M. Rajamathi, *Carbon*, 2008, **46**, 1773–1781.
- 49 B. J. Li, H. Q. Cao, J. Shao and M. Z. Qu, *Chem. Commun.*, 2011, **47**, 10374–10376.
- 45 50 C. N. He, S. Wu, N. Q. Zhao, C. S. Shi, E. Z. Liu and J. J. Li, *ACS Nano*, 2013, **7**, 4459–4469.
- 51 C. R. Brundle, T. J. Chuang and K. Wandelt, *Surf. Sci.*, 1977, **68**, 459–468.
- 50 52 J. Lu, X. L. Jiao, D. R. Chen and W. Li, *J. Phys. Chem. C*, 2009, **113**, 4012–4017.
- 53 D. W. Wang, F. Li, M. Liu, G. Q. Lu and H. M. Cheng, *Angew. Chem. Int. Ed.*, 2008, **47**, 373–376.
- 54 S. B. Yang, G. L. Cui, S. P. Pang, Q. Cao, U. Kolb, X. L. Feng, J. Maier and K. Müllen, *Chem. Sus. Chem.*, 2010, **3**, 236–239.
- 55 55 V. S. Zaitsev, D. S. Filimonov, I. A. Presnyakov, R. J. Gambino and B. Chu, *J. Colloid Interface Sci.*, 1999, **212**, 49–57.
- 56 X. Du, C. Wang, M. Chen, Y. Jiao and J. Wang, *J. Phys. Chem. C*, 2009, **113**, 2643–2646.
- 60 57 Q. H. Wang, L. F. Jiao, H. M. Du, Y. J. Wang and H. T. Yuan, *J. Power Sources*, 2014, **245**, 101–106.
- 58 J. P. Cheng, Q. L. Shou, J. S. Wu, F. Liu, V. P. Dravid and X. B. Zhang, *J. Electroanal. Chem.*, 2013, **698**, 1–8.
- 59 W. H. Shi, J. X. Zhu, D. H. Sim, Y. Y. Tay, Z. Y. Lu, X. J. Zhang, Y. Sharma, M. Srinivasan, H. Zhang, H. H. Hng and Q. Y. Yan, *J. Mater. Chem.*, 2011, **21**, 3422–3427.
- 65

Cite this: DOI: 10.1039/c0xx00000x

www.rsc.org/materials

PAPER

## Table of Content Graphic



Superior behavior for supercapacitors highlight the potential applications of CFGC in energy storage issues.